Precipitation of silica from zinc process solution

Tuomas Vielma[1] ● Ulla Lassi[2] ● Justin Salminen[3]

Received: ……/Accepted …

Abstract Precipitation of silica during hot acid leach of zinc residue was studied with laboratory-scale batch experiments. It was observed that the high ionic strength of the leaching solution drastically decreases the solubility of silica. The solubility was also studied by Gibbs energy minimization method using the software ChemSheet. Good agreement was obtained between the model and experimental results. The precipitation reaction was observed to follow a pseudo-first order rate-law. Effects of initial silicic acid concentration, temperature and sulfuric acid concentration were studied. Based on the used rate-law, an activation energy of 61,7 kJ mol^{-1} was estimated, implying a reaction-controlled mechanism of precipitation.

Keywords Kinetics ● Thermodynamics ● Zinc ● Silica ● Salt effect ● Solubility

✉ Tuomas Vielma
tuomas.vielma@chydenius.fi
[1] Tuomas Vielma, University of Oulu, Oulu, Finland

[2] Justin Salminen, affiliation of second author

[3] Ulla Lassi, University of Oulu, Oulu, Finland

Introduction

Gelling of silicic acid is a widely-recognized problem in hydrometallurgical recovery of zinc. Acid leaching of silicate minerals such as willemite $Zn_2SiO_4(s)$ and hemimorphite $Zn_4Si_2O_7(OH)_2 \cdot H_2O(s)$ liberates various silicic acid species into the process solution [1], in accordance with equations 1 and 2:

$$Zn_2SiO_4(s) + 4H^+(aq) \Leftrightarrow 2Zn^{2+}(aq) + Si(OH)_4(aq) \quad (1)$$

$$Zn_4Si_2O_7(OH)_2 \cdot H_2O(s) + 8H^+(aq) \Leftrightarrow 4Zn^{2+} + Si_2O(OH)_6(aq) + 3H_2O \quad (2)$$

At high concentrations polymerization and gelling of silicic acid can be observed. This leads to difficulties with settling, filtering and washing of the process solution and may even hinder the leaching process itself. Due to its slow sedimentation velocity, silicic acid gel is practically impossible to separate from the solution in a thickener. Formation of the gel can thus hinder the operation of later stages, including hot acid leach and electrowinning [1-6].

Due to its status as a global problem in hydrometallurgy of zinc, many attempts have been made to control the precipitation and gelling of silicic acid. Several patents have been issued for processes capable of processing silica bearing raw material. The Radino process was one the earliest attempts, later improved by Matthew and Elsner [3,7,8]. Key idea of the process is to, after leaching of the raw material, neutralize the leaching solution with ZnO to pH of 4-5 where colloidal silica is most unstable [9]. Temperature is maintained at 50-60 °C to prevent uncontrolled precipitation of silica and loss of zinc. Precipitated silica is separated by filtration. Aluminium sulfate is added to increase the rate of precipitation of silica. Although the modified Radino process can handle high silica concentrations, a sudden halt at the process can cause uncontrollable gelling of silica with detrimental results for the whole process chain. To tackle this problem, the Outokumpu process was developed [10].

Whereas the modified Radino process relied on multiple successive reactors, Outokumpu process was developed for a single reactor. The process was designed to precipitate silica at the same rate silica bearing material is introduced to the process. High acid concentration, 20 – 100 g H_2SO_4 dm^{-3}, and high operation temperature, 70 °C, are used to ensure complete dissolution of silicates. By maintaining silica concentration at 0.5 – 2.0 g SiO_2 dm^{-3}, easily filterable precipitate is obtained. Similar concentration

limits have been found by other parties [11]. Clear advantages of Outokumpu process are also the simplicity of the necessary facilities and their operation [10].

As was pointed out by Cooper, processes designed to treat silicate-bearing zinc concentrates were created when the knowledge of the solution behavior and precipitation of silicic acid was still lacking [11]. In the systems considered here, solubility of silicic acid is controlled by the solubility equilibrium of amorphous silica, shown in equation 3:

$$\mathrm{SiO_2(am) + 2H_2O(l) \Leftrightarrow Si(OH)_4(aq)} \quad (3)$$

Precipitation of amorphous silica instead of more stable quartz can be considered as a manifestation of Ostwald's rule of stages. The equilibrium constant of reaction 3 and solubility of amorphous silica are related through equation

$$K = \frac{a_{\mathrm{Si(OH)_4}}}{a_{\mathrm{H_2O}}{}^2} \quad (4)$$

where $a_{\mathrm{Si(OH)4}}$ is the equilibrium activity of silicic acid and a_{H2O} is the equilibrium activity of water. At infinite dilution, the equilibrium constant

approaches the solubility of silica. At room temperature K is on the order of 10^{-3} M, but the solubility is heavily affected by temperature [12] and presence of electrolytes in the solution [13]. Increase in temperature increases the solubility, whereas increase in ionic strength decreases it. This due to increased hydration energy of silica as the activity of water decreases [14].

Precipitation of silica proceeds via polymerization of monomeric silicic acid units. Initially short linear structures are formed, which then condense to small ring-like polymers. Internal condensation of the cyclic silicic acid molecules leads to formation of small spherical nanoparticles that also act as nuclei for the precipitation. In acidic solutions, pH < 2, polymerization proceeds mainly by addition of monomeric silicic acid to larger polymers [15]. It is known that particles suspended in a solution can grow by Ostwald ripening, ie. dissolution of smaller, more soluble particles and the following deposition on larger particles [16]. Rate of the ripening process is controlled by the solubility of the bulk matter [17]. As is shown in this work, however, high ionic strength of the solution decreases the already low solubility of silica, and in the short time-scale of the precipitation, Ostwald ripening is likely to be negligible.

Precipitation process continues with aggregation of polymerized silica particles. It was shown by Cooper [11] that initial silicic acid concentration and supersaturation state control the precipitation product, both in batch and continuous precipitation. At low supersaturation, solid well filterable aggregates form. Increasing the initial silicic acid concentration leads to formation micro-gel, gelatinous particles that also hinder the filterability. Even higher supersaturation leads to formation of silicic acid gel.

Kinetics of the polymerization and precipitation process have been considered by multiple authors, but there are large discrepancies between reported kinetic regimes. Reaction rates varying in order from 1 to 5 with respect to dissolved silicic acid have been reported, on some occasions with a change in order as a function of pH [18-29]. Although some studies have been made at low to extremely low pH values, based on our literature survey, no studies have considered the high ionic strengths typically met in hydrometallurgical processes. Most of the studies on silica precipitation kinetics have focused on simple systems of geochemical interest.

Results and Discussion

The thermodynamic calculation software ChemSheet was used in this work to model the solubility of silica in concentrated metal sulfate solutions [30]. ChemSheet provides a flexible spreadsheet interface powered by a

ChemApp-based Gibbs energy minimization routine. The excess Gibbs energies of the solute species were modelled with the Pitzer model using temperature-dependent parameters. The neutral-ion interaction parameters between aqueous silica and solute ions, $\lambda_{SiO2\text{-}j}$, were approximated from the effective electrostatic radii of the ions using equations presented by Azaroual et al [31] and Accornero & Marini [32], who showed that for many metal cations there exists a clear relationship between $\lambda_{SiO2\text{-}j}$ and the cations effective electrostatic radii. The electrostatic radii were calculated from the equations presented by Shock et al [33]. Exceptions were $\lambda_{SiO2\text{-}SO4}$ and $\lambda_{SiO2\text{-}H}$, for which the data was taken directly from Azaroual et al [31].

Fig. 1 shows solubility of silica in pure water as predicted by ChemSheet as a function of temperature. Values collected from literature are shown for comparison [12,34-36]. As can be seen, agreement between the model and the reported values is good. Solubility predicted by the regression equation of Gunnarsson & Arnórsson is also shown [12]. The two curves agree within the uncertainty of presented measurements. Fig. 2 shows the correlation between calculated and measured solubilities both in pure water and electrolyte solutions. Data shown is from this work and from literature [12,37,38]. Results from this work were also included. Again, the

correlation is good in general, even though concentrated electrolyte solutions were included.

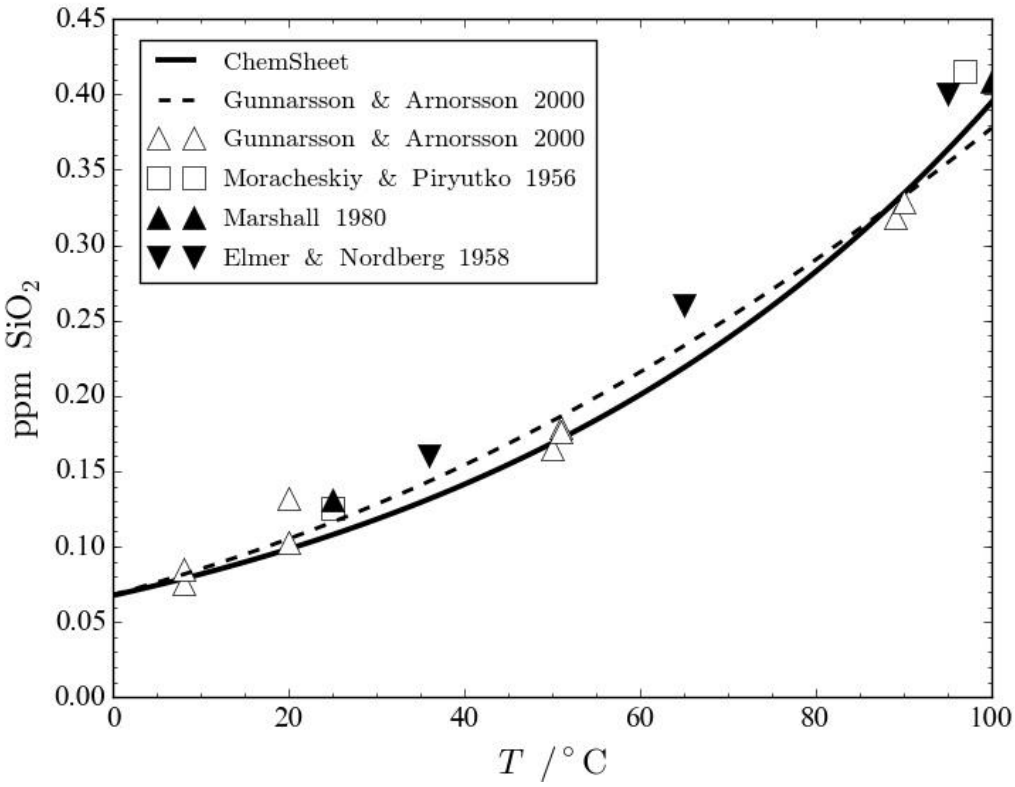

Fig. 1 Solubility of silica as a function of temperature. Values calculated with ChemSheet compared to values collected from literature [12,34-36].

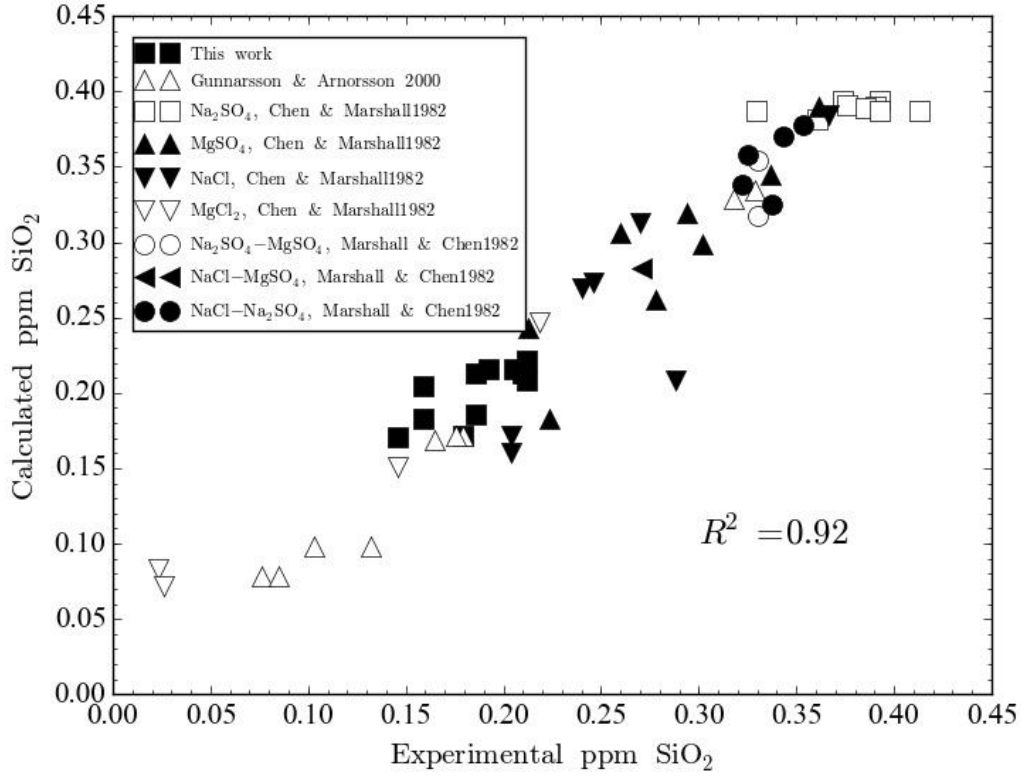

Fig. 2 Correlation between measured and calculated solubilities. Data from this work and literature [12,37,38].

Based on our measurements, at the operating conditions of the hot acid leach, solubility of silica is lowered to approximately one half of that in pure water, ie. approximately 200 ppm. This due to the high electrolyte content of the solution. Presence of electrolytes decreases the activity of water and interferes with the hydration of silica, effectively lowering its solubility. A rather clear relationship can be observed between the ionic strength of the solution, calculated from the measured concentrations, and the solubility of silica. Fig. 3 shows solubility of silica in metal sulfate

solutions as a function of ionic strength. Figure includes results from this work and from Chen & Marshall [37], Gunnarsson & Arnórsson [12] and Cooper [11]. Salting-out of silica is apparent. The solid curve was calculated with ChemSheet using different levels of dilution for the average composition of solutions used in this work. The model results moderately agree with the experimental results. The solubility is to some degree independent of the specific composition of the solution. This is most likely because the ionic strength is mostly defined by zinc and sulfate ions, the two most abundant components. It should also be noted that the neutral-ion interaction coefficients were of similar magnitude for all considered metals. This implies that ionic strength of the metal sulfate containing process solutions can be used as an indicator for the solubility of silica.

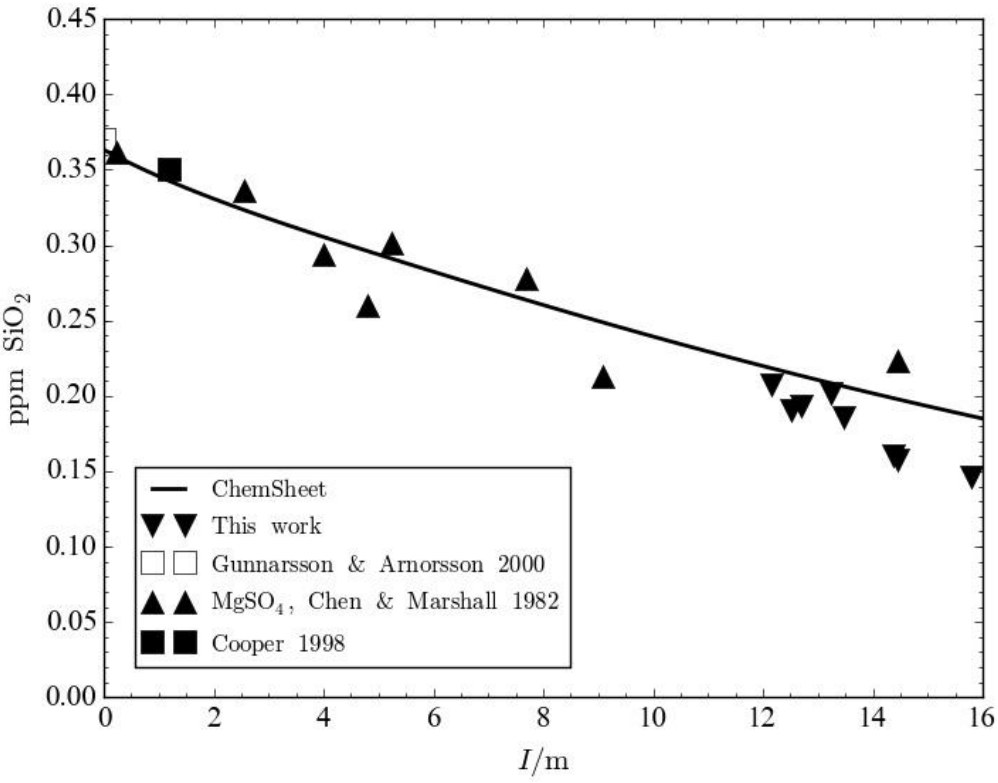

Fig. 3 Solubility of silica in metal sulfate solutions as function of ionic strength. Results from Chen & Marshall [37] at 100 °C, others at 95 °C [11]. □ was calculated from the equation presented by Gunnarsson & Arnórsson [12].

Concentration of soluble silica was followed on regular intervals during all the precipitation experiments. Fig. 4 shows the typical precipitation curve for model solutions. An induction period, during which the concentration of soluble silica decreases rather slowly, is observed for the first 20 h. This is followed by a more rapid precipitation phase, and in 5-6 h silica concentration reaches equilibrium level. The shape and timescale of these precipitation curves agree well with results of Cooper [12]. However, the

solubility level is much lower than the 350 ppm SiO_2 reported, most likely due to the higher ionic strength as the calculations above showed.

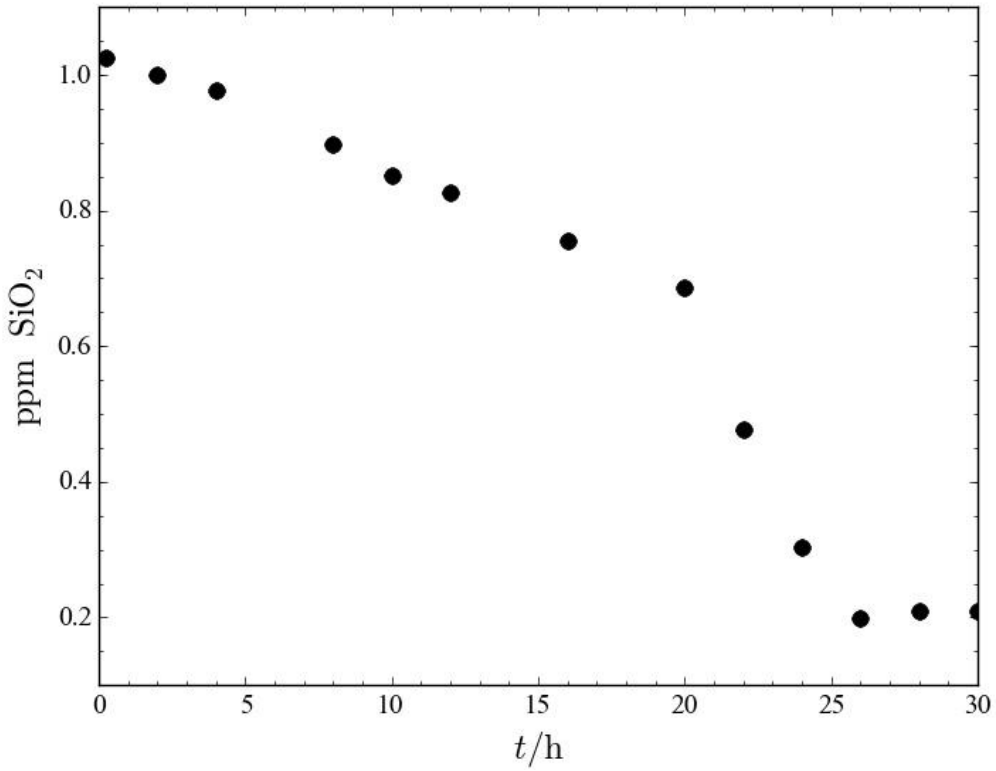

Fig. 4 Precipitation curve of silica for a synthetic solution. Note the almost linear decrease in soluble silica concentration during the induction period.

For the authentic solutions, no induction period was observed. This could be caused by the pre-existing silica nuclei and suspended solids in the solution. Thus the nucleation phase is circumvented by direct deposition of soluble silica on the existing active surfaces. This leads to only an exponential decay of silicic acid concentration towards equilibrium concentration being observed. The exponential decay implies a kinetic

regime first order with respect to soluble silica. This is in agreement with the fact that growth of colloidal silica particles is of the first order with respect to monomeric silicic acid [39]. Weres et. al observed that increase in ionic strength increases the rate of particle growth and precipitation, and concluded it was due to change in degree of surface protonation [29]. From our results, however, no clear relationship between precipitation rate and ionic strength could be established.

Equation 5 shows the rate-law used to model the kinetics of silica precipitation.

$$\frac{dc_{\mathrm{Si(OH)_4}}}{dt} = k(c^{*}_{\mathrm{Si(OH)_4}} - c_{\mathrm{Si(OH)_4}}) \quad (5)$$

Solution of differential equation 5 is given by equation 6.

$$c_{\mathrm{Si(OH)_4}}(t) = (c_0 - c^{*}_{\mathrm{Si(OH)_4}})e^{-kt} + c^{*}_{\mathrm{Si(OH)_4}} \quad (6)$$

Equation 6 was fitted to the experimental data using a non-linear fitting algorithm. Goodness of fit and the applicability of the model was judged by analysis of residuals and calculated R^2 values. Reaction rate constant k,

initial silicic acid concentration c_0 and equilibrium concentration c^* were taken as the fitting parameters. In general, the obtained fit was excellent.

Effect of silicic acid concentration

Effect of initial silicic acid concentration was investigated by adding synthetic willemite and a stoichiometric amount of sulfuric acid to authentic process solutions at the start of experiment. The initial concentrations were 0.524, 0.736 and 2.328 g SiO_2 dm^{-3}. It was observed that at low concentrations, the precipitation reaction follows the proposed rate law. At higher concentration, however, the precipitation somewhat deviates from this behavior, and possibly a short induction phase is observed. The latter part of the precipitation curve provided an acceptable fit to the proposed rate law. However, the fit resulted to considerably larger reaction rate constant (0.285 s^{-1}) than for the lower initial concentrations (on average 0.085 s^{-1}). Precipitation curves for different initial silica concentrations are shown in Fig. 5.

The induction phase was observed likely due to the large amount of added willemite. High concentration of silicic acid is liberated, leading to similar set-up as in the experiments with model solutions. The decrease in silicic acid concentration during the induction phase, however, was much more rapid than in the model solutions. This is could be due to pre-existing silica

nuclei and other suspended solids, that allow for heterogenous nucleation to take place. It is also interesting to note that regardless of the measured initial silicic acid concentration, solubility level was achieved in approximately 6 h.

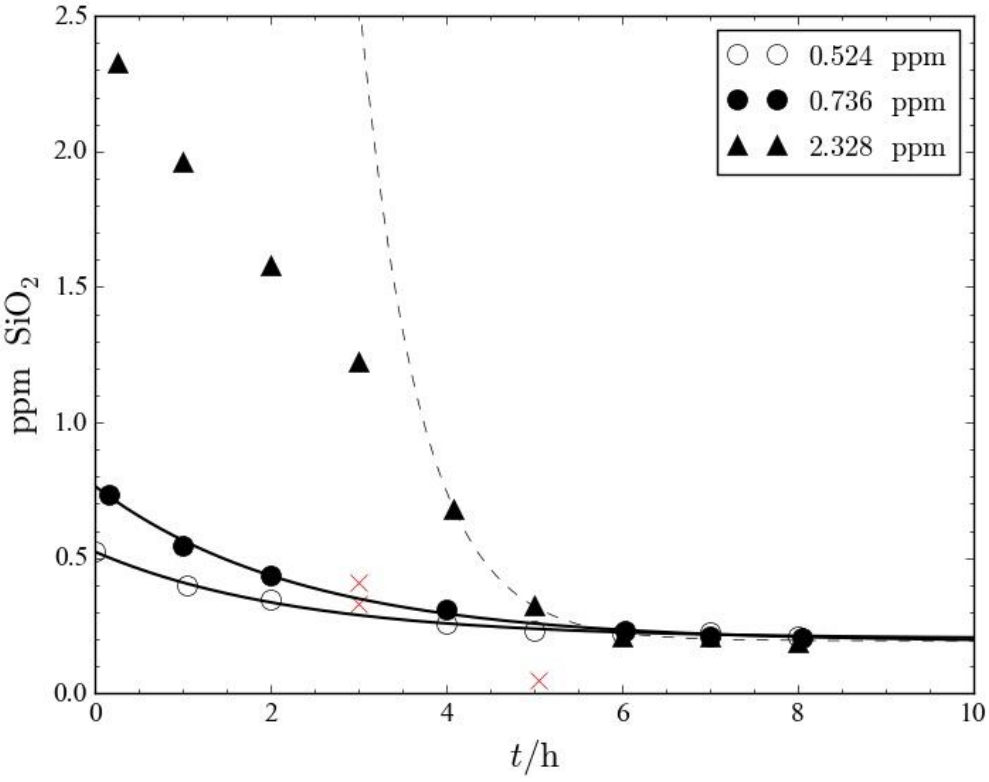

Fig. 5 Precipitation curves with varying initial concentration of soluble silica. -- is the fit to the latter part of precipitation curve with initial silica concentration of 2.328 ppm.

Effect of sulfuric acid concentration

A set of experiments was performed to study the effect of sulfuric acid concentration on the rate of precipitation. Experiments were carried out with 75 and 100 g H_2SO_4 dm^{-3}. Fig. 6 shows comparison between the measured precipitation curves.

It is known that at low pH, protons catalyze the polymerization reaction of silicic acid and precipitation of silica, and increase in acid concentration increases the rate of precipitation and gelling at low pH [11,40,41]. A linear relationship was observed between sulfuric acid concentration and reaction rate constant *k*, on the investigated concentration range. The results are presented graphically in Fig. 7. Our result is in stark contrast with literature, since Gorrepati et al reported an exponential relationship between hydrochloric acid concentration and reaction rate [41]. Hurd & Barclay reported an exponential relationship between sulfuric acid concentration and reaction rate constant [40]. This can be partly due to different kinetic models used; Hurd & Barclay calculated reaction rate constant as the inverse of precipitation time, and Gorrepati et al used a model based on a fast second order polymerization followed by a aggregation step modelled with Smoluchowksi equation.

1

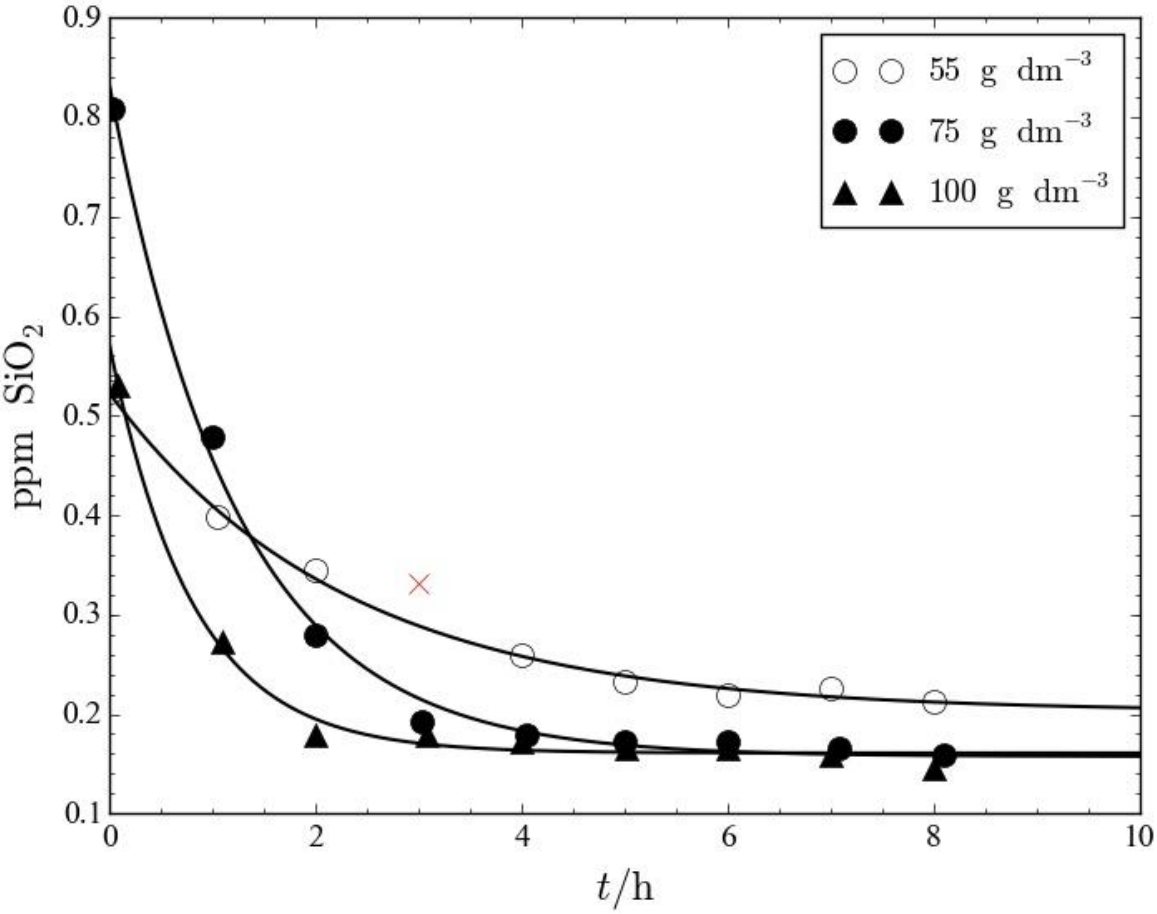

Fig. 6 Precipitation curves with varying sulfuric acid concentrations.

2

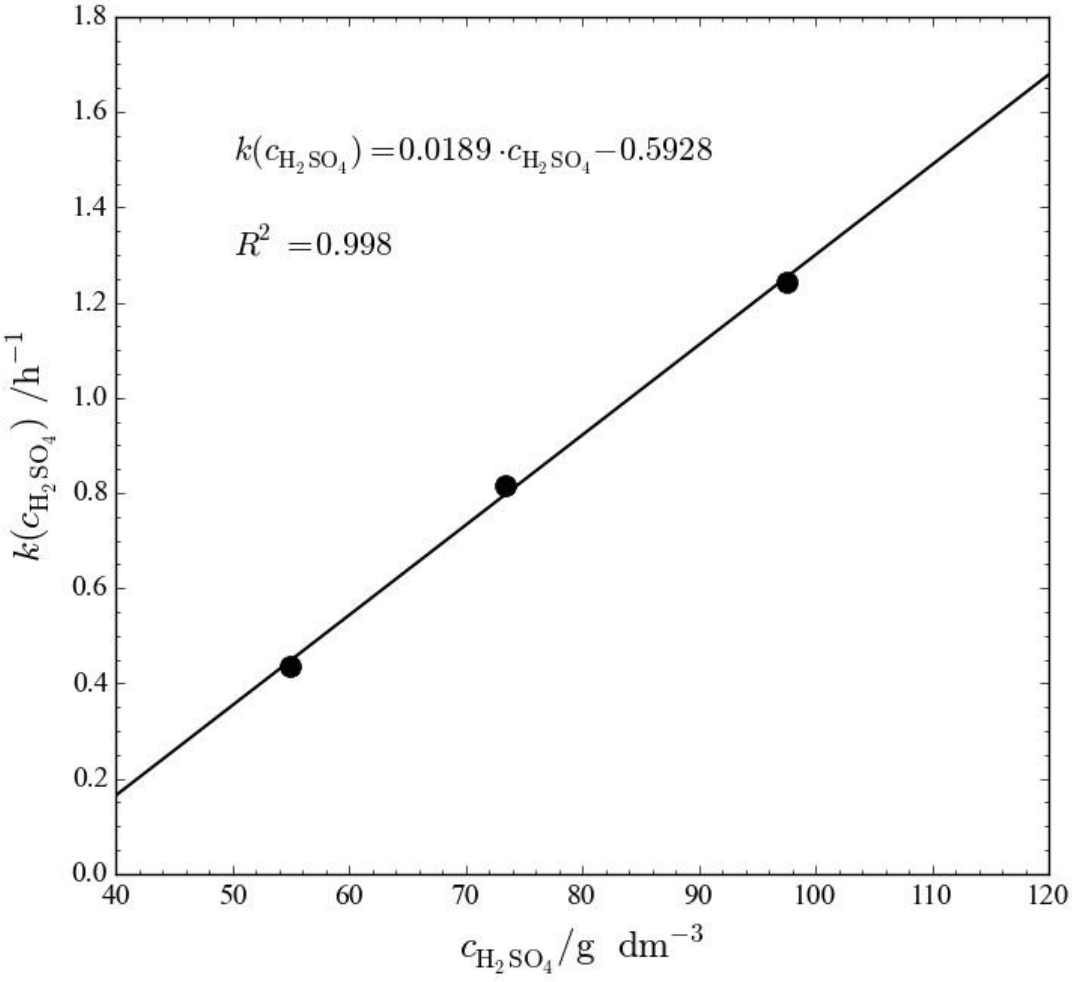

Fig. 7 A linear relationship was observed between the reaction rate constant *k* and sulfuric acid concentration.

1 .

2 **Activation energy of precipitation**

3 Precipitation experiments were performed at temperatures 80, 85, 90, 95

4 and 100 °C. Precipitation curves at 90, 95 and 100 °C are shown in Fig 8.

5 At 80 °C, an induction phase was observed, and the experiment was

terminated before rapid precipitation had occurred. High initial silicic acid concentration, 2.0 g dm^{-3}, was also measured. The high silicic acid concentration, as explained above, together with the lowered temperature most likely lead to slow nucleation and an observable induction phase. It is left for further studies to find the relative importance of these two factors.

Irregularities were observed, when drawing the Arrhenius plot. Reaction rate constant was higher at 85 °C than at 90 or 95 °C. It was excluded from the data set, but this lead to abnormally high apparent activation energy of 196 kJ mol^{-1}. The fit for the data at 100 °C was also not satisfactory. After excluding the rate constant at 100 °C, a value of 61.7 kJ mol^{-1} was obtained. The value is a crude estimate since it was calculated essentially based on just two temperatures. It, however, points towards a reaction-controlled mechanism for the precipitation reaction. This agrees with the fact that silica solutions are kinetically stable at low pH, a diffusion-controlled mechanism is thus unlikely. It is also comparable to values previously reported in the literature; 61 kJ mol^{-1} by Carrol et. al [42], 54.8 kJ mol^{-1} by Fleming [43] and 49.8 kJ mol^{-1} by Rimstidt and Barnes [44], but it should be mentioned that these observation were made for entirely different solution media. Fig. 9 shows the Arrhenius plot.

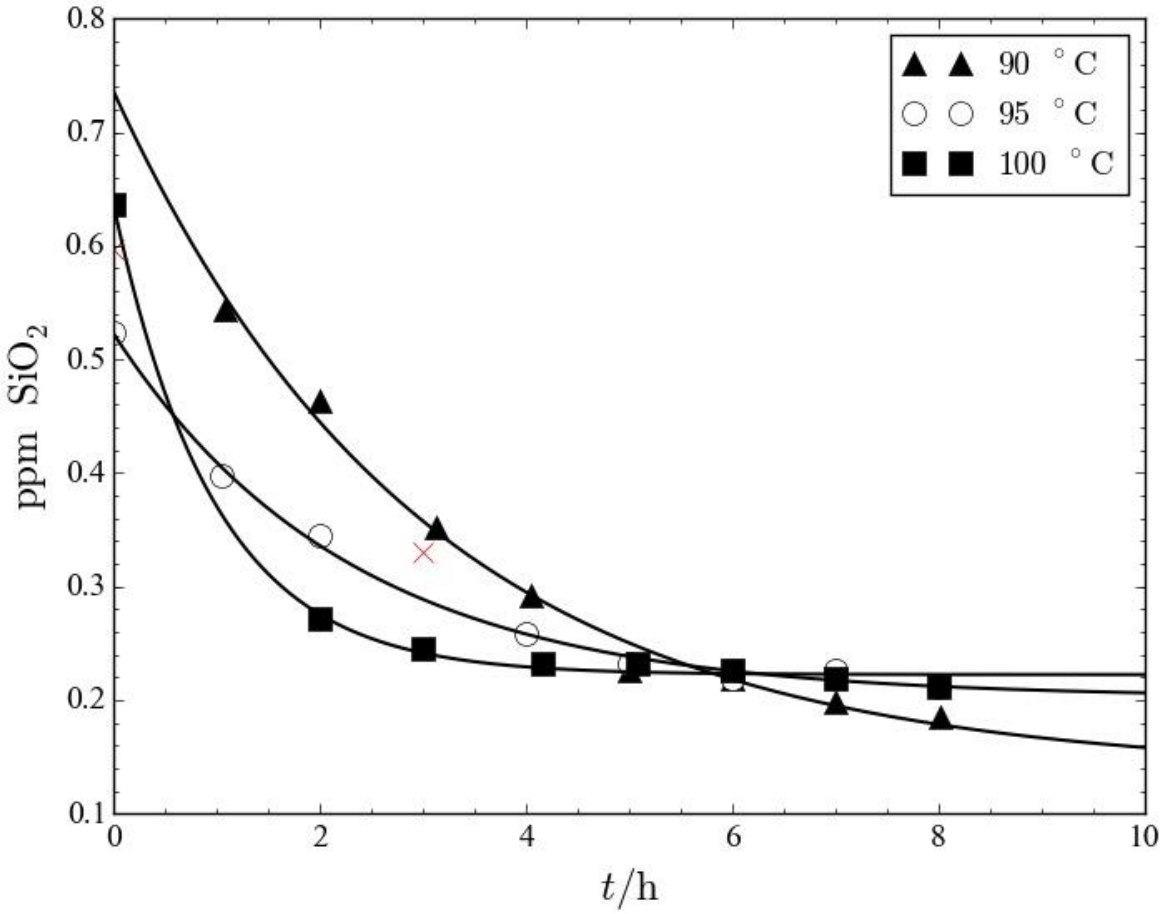

Fig. 8 Precipitation curves measured at 90, 95 and 100 °C.

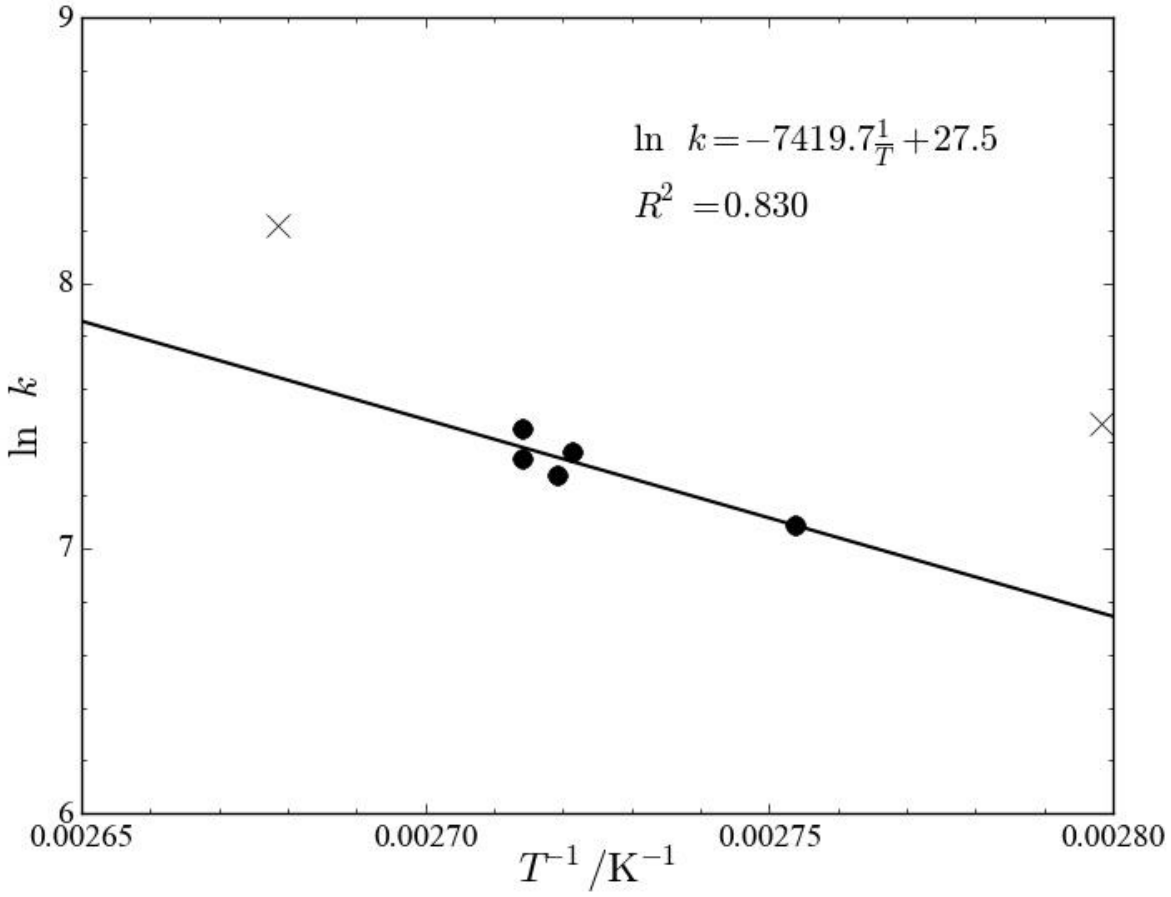

Fig. 9 Arrhenius plot for the precipitation of silica. × are the rejected data points (see for text).

1 Conclusions

2 This work has several implications for hydrometallurgic industry. Behaviour
3 of aqueous silica is greatly altered by high concentrations of soluble metals.
4 During hot acid leach of zinc minerals, solubility of silica is approximately
5 half of that in pure water. This leads easily to high supersaturation and
6 gelling. Under normal operating conditions, precipitation is complete in

approximately 5-6 hours. By increasing the acid concentration or solution temperature, it possible to complete the precipitation in only 1-2 hours. Good agreement was achieved between experimental data and the thermodynamic and kinetic models. It appears that ionic strength calculated from the solution composition can be used to predict silica solubility. Based on pseudo-first order rate law, apparent activation energy of precipitation was estimated to be 61.7 kJ mol^{-1}, which is in moderate agreement with the literature and suggests a reaction-controlled mechanism for precipitation of silica.

Experimental

Materials

Willemite used in this work was synthesised from ZnO (≥99.0 %, Sigma-Aldrich), SiO_2 (purum p.a., Sigma-Aldrich) and NaOH (≥99.0 %, Merck). Model solutions were made by dissolving reagent grade metal sulfates into a sulfuric acid solution that was then diluted to volume of 0.9 dm^3. Reagents used in this work were $Al_2(SO_4)_3 \cdot 16H_20$ (≥95.0 %, Fluka Analytical), $Fe_2(SO_4)_3 \cdot xH_2O$ (21-23 % Fe, Sigma-Aldrich), $MgSO_4 \cdot 7H_2O$ (≥99.5 %, Oy FF-Chemicals Ab), $MnSO_4 \cdot H_2O$ (≥99.0 %, Sigma-Aldrich), $ZnSO_4 \cdot 7H_2O$ (≥99.0 %, Sigma-Aldrich), H_2SO_4 (95.0 %, Merck). Authentic solutions were obtained from a local zinc plant.

Apparatus

A custom-made baffled stainless steel reactor was used as the reaction vessel. Operating volume of the reactor was 1 l. A pitched-blade impeller with a ball-bearing was fitted through the reactor's lid along with a reflux condenser, to prevent evaporation of the solution without build-up of pressure. Air was bubbled through a vent at the bottom of the vessel to ensure slightly oxidative environment. pH and RedOx-meter were used to monitor the pH and reduction potential during precipitation. Temperature was measured with a standard digital thermometer. The range of experimental conditions covered in this work are presented in Table 1.

Table 1. Range of experimental conditions.

Temperature	80 – 100 °C
Stirring speed	250 rpm
Air flow	0.5 dm^3 min^{-1}
Sulfuric acid concentration	55 – 100 g H_2SO_4 dm^{-3}

Willemite synthesis

Willemite was synthesised by a sol-gel reaction followed by calcination. A modified version of the method presented by Yatabe et al. was used [11, 45].

A solution of sodium silicate was slowly added to acidic solution of zinc sulfate. A thick white precipitate formed, which was then left to settle for 24 h. It was then separated from the solution, washed twice and dried over night at 105 °C. Dried precipitate was calcined at 1100 °C for 12 h to transform the amorphous zinc silicate to crystalline willemite.

Cooled product was washed twice with aqueous sodium hydroxide solution to dissolve any excess silicon dioxide. After filtering and washing with distilled water the product was dried at 105 for 24 h. The final product was characterised with XRPD. No major impurities were identified. The synthesised willemite was ball-milled before use.

Experiments with model solutions

An acidic metal sulfate solution was prepared from the reagents. The solution was heated in the reactor to the target temperature. Fine ground willemite was added and timer started. Samples were taken regurarly and filtrated through a 0.45 μm syringe filter. Filtered samples were immediately diluted with dilute sulfuric acid solution. Samples were analyzed later with ICP-OES for Si, Zn, Fe, Al, Mn and Mg. pH, temperature and RedOx-potential were measured regurarly. It is important to note that the measure of soluble silica in this work was the total concentration that would pass the 0.45 μm filter.

Experiments with authentic solutions

The authentic solutions used were fresh from the process. The reaction vessel was pre-heated to minimize the delay between taking the solution and starting the experiment. After the solution inside the reactor reached target temperature zone, timer was started. Possible additives, willemite or sulfuric acid, were added at this point. Sampling was again done regularly, in the same manner as described above. After terminating the experiment, the processed solution was filtrated.

Acknowledgements

References

[1] Terry B (1983) Hydrometallurgy **10:** 135

[2] Terry B (1983) Hydrometallurgy **10:** 151

[3] Matthew IG, Elsner D (1977) Metall Trans B **8:** 73

[4] Safari V, Arzpeyma G, Rashchi F, Mostoufi N (2009) Int J Miner Process **93:** 79

[5] Ikenobu S, Shimokawa K (1998) Method for processing zinc

silicate-containg zinc crude material. European Patent 0 851 034 A1, Jul 1, 1998

[6] Dufresne RE (1976) JOM **28:** 8

[7] Radino HL (1957) Process of zinc extraction from ores comprising soluble silicates by means of hydrometallurgy. Australian Patent 224,195.

[8] Perry W (1966) Chem Eng **73:** 182

[9] Queneau PB, Berthold CE (1986) Can Metall Q **25:** 201

[10] Fugleberg SP, Poijärvi JTI (1979) Hydrometallurgical treatment of soluble silicate-bearing zinc materials. US Patent 4,148,862 A.

[11] Cooper RMG (1998) *Silica precipitation from electrolytic zinc solutions*. Ph.D. dissertation. Curtin University of Technology, Australia, 1998.

[12] Gunnarsson I, Arnórsson S (2000) Geochim Cosmochim Acta **64:** 2295

[13] Marshall WL, Chen CTA (1982) Geochim Cosmochim Acta

46: 289

[14] Dove PM, Rimstidt JD (1994) In: Silica: Physical Behavior, Geochemistry and Material Applications. American Mineral Society.

[15] Shimada K, Tarutani T (1979) J Chromatogr **168:** 4017

[16] Ostwald W. (1896) Lehrbuch der Allgemeinen Chemie. Leipzig, Germany.

[17] Wagner, C (1961) Z Elektrochem **35:** 581

[18] Alexander GB (1954) J Am Chem Soc **76:** 2094

[19] Baumann H (1959) Kolloid Z **162:** 28

[20] Bishop AD, Bear JL (1972) Thermochim Acta **3:** 399

[21] Conrad CF, Yasuhara H, Bandstra JZ, Icopini GA, Brantley SL, Heaney PJ (2007) Geochim Cosmochim Acta **71:** 531

[22] Crerar D, Axtmann EV, Axtmann RC (1981) Geochim Cosmochim Acta **45:** 1259

[23] Goto K (1956) J Phys Chem 60: 1007

[24] Icopini GA, Brantley SL, Heaney PJ (2005) Geochim

Cosmochim Acta 69: 293

[25] Kitahara S (1960) Rev Phys Chem Jpn 30: 131

[26] Makrides AC, Turner M, Slaughter J (1980) J Colloid Interface Sci **73:** 345

[27] Okamoto G, Okura T, Goto K (1957) Geochim Cosmochim Acta **12:** 123

[28] Rothbaum HP, Rhode AG (1979) J Colloid Interface Sci **71:** 533

[29] Weres O, Yee A, Tsao L (1981) J Colloid Interface Sci **84:** 379

[30] Koukkari P, Penttilä K, Hack K, Petersen S (2000) In: Microstructures, Mechanical Properties and Processes Computer Simulation and Modeling. Wiley-VHC, Weinheim.

[31] Azaroual M, Fouillac C, Matray JM (1997) Chem Geol 140: 155

[32] Accornero M, Marini L (2009) Appl Geochem **24:**747

[33] Shock EL, Oelkers EH, Johnson JW, Sverjensky DA, Helgeson HC (1992) J Chem Soc Faraday Trans **88:** 803

[34] Morachevskiy YV, Piryutko MM (1956) Russ Chem Bull **5:** 917

[35] Marshall W (1980) Geochim Cosmochim Acta **44:** 907

[36] Elmer TH, Nordberg ME (1958) J Amer Ceram Soc **41:** 517

[37] Chen CTA, Marshall W (1982) Geochim Cosmochim Acta **46:** 279

[38] Marshall W, Chen CTA (1982) Geochim Cosmochim Acta **46:** 289

[39] Tobler DJ, Shaw S, Liane GB (2009) Geochim Cosmochim Acta **73:** 5377

[40] Hurd CB, Barclay RW (1940) J Phys Chem **44:** 847

[41] Gorrepati EA, Wongthahan P, Raha S, Fogler HS (2010) Langmuir **26:** 10467

[42] Carroll S, Mroczek E, Alai M, Ebert M (1998) Geochim Cosmochim Acta **62:** 1379

[43] Fleming BA (1986) J Colloid Interface Sci **110:** 40

[44] Rimstidt JD, Barnes, HL (1980) Geochim Cosmochim Acta

110: 40

[45] Yatabe J, Yamada S, Ikawa T, Kageyama T (1992) Nippon Kagaku Kaishi **5:** 565

Following the References section, *Figure Captions* (separated from the actual figures), *Tables*, *Schemes*, and *Figures* should be collected to facilitate the production process.

Figure Captions

Fig. 1 Solubility of silica as a function of temperature. Values calculated with ChemSheet compared to values collected from literature [12,34-36].

Fig. 2 Correlation between measured and calculated solubilities.

Fig. 3 Solubility of silica in metal sulfate solutions as function of ionic strength. Results from Chen & Marshall [37] at 100 °C, others at 95 °C [11].

Fig. 4 Precipitation curve of silica for a synthetic solution. Note the almost linear decrease in soluble silica concentration during the induction period.

Fig. 5 Precipitation curves with varying initial concentration of soluble silica.

Fig. 6 Precipitation curves with varying sulfuric acid concentrations.

Fig. 7 A linear relationship was observed between the reaction rate constant *k* and sulfuric acid concentration.

Fig. 8 Precipitation curves measured at 90, 95 and 100 °C.

Fig. 9 Arrhenius plot for the precipitation of silica. × are the rejected data points (see for text).

Table 1. Range of experimental conditions.

Temperature	80 – 100 °C
Stirring speed	250 rpm
Air flow	0.5 dm^3 min^{-1}
Sulfuric acid concentration	55 – 100 g H_2SO_4 dm^{-3}

Figure 1

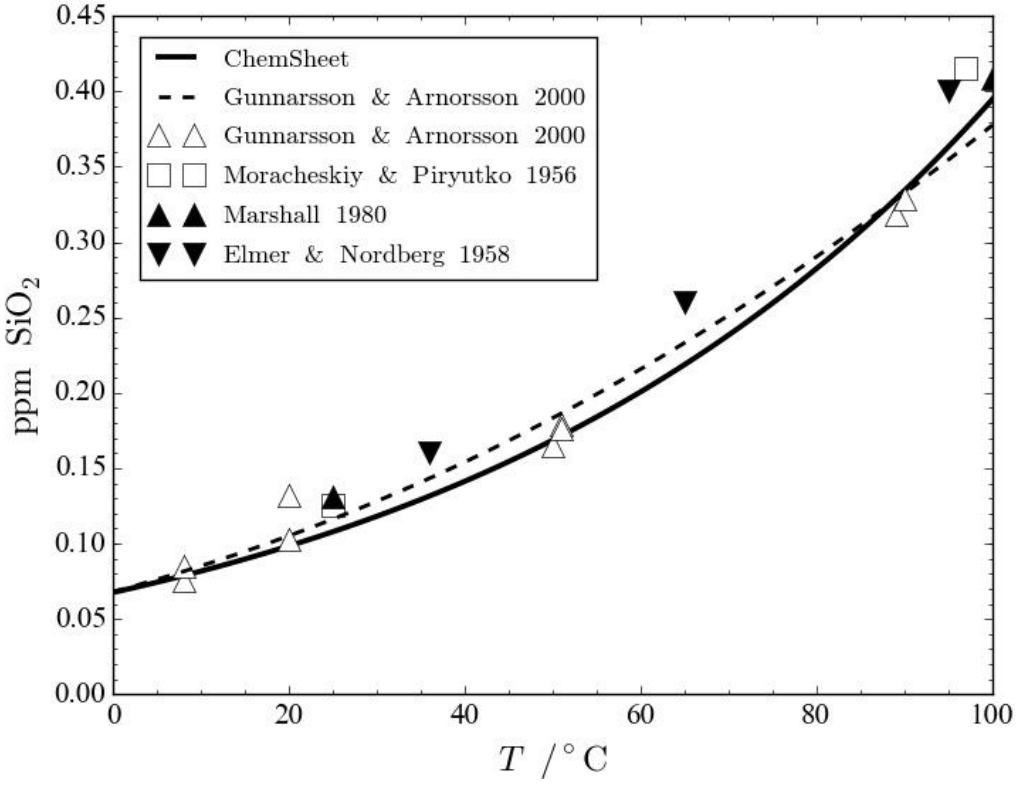
ChemSheet
Gunnarsson & Arnorsson 2000
Gunnarsson & Arnorsson 2000
Moracheskiy & Piryutko 1956
Marshall 1980
Elmer & Nordberg 1958
ppm SiO2
T / °C
0.45
0.40
0.35
0.30
0.25
0.20
0.15
0.10
0.05
0.00
0
20
40
60
80
100

Figure 2

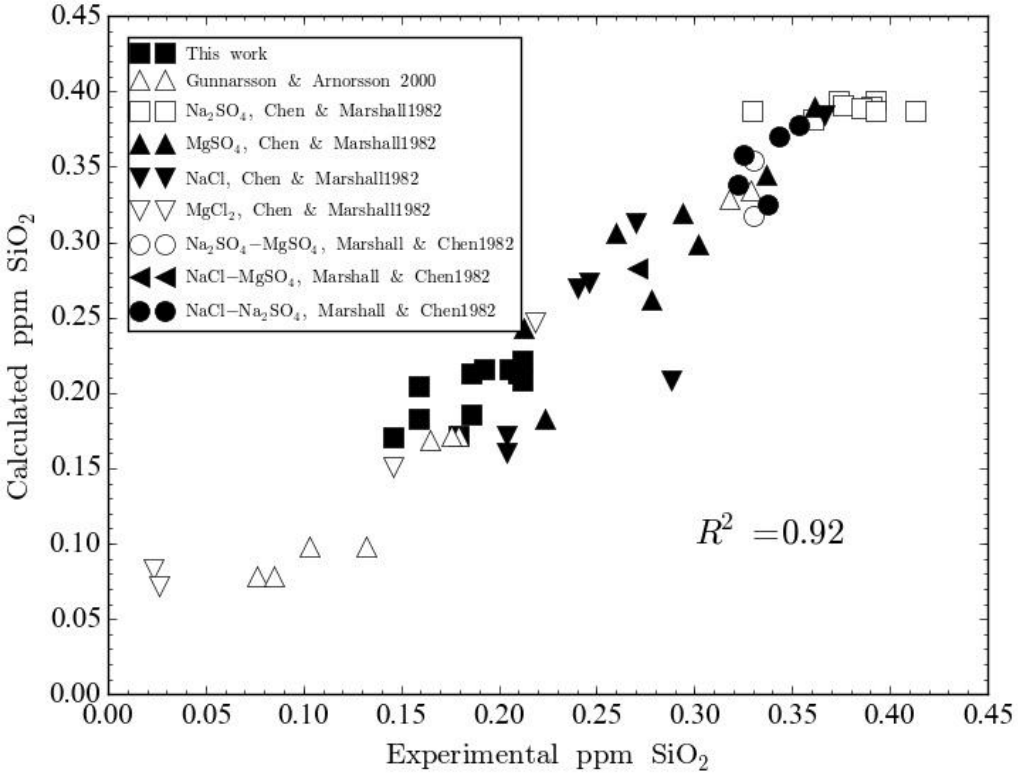
This work
Gunnarsson & Arnorsson 2000
Na_2SO_4, Chen & Marshall1982
$MgSO_4$, Chen & Marshall1982
NaCl, Chen & Marshall1982
$MgCl_2$, Chen & Marshall1982
$Na_2SO_4-MgSO_4$, Marshall & Chen1982
$NaCl-MgSO_4$, Marshall & Chen1982
$NaCl-Na_2SO_4$, Marshall & Chen1982
R^2 =0.92
Calculated ppm SiO_2
Experimental ppm SiO_2
0.00
0.05
0.10
0.15
0.20
0.25
0.30
0.35
0.40
0.45

1

2

3

Figure 3

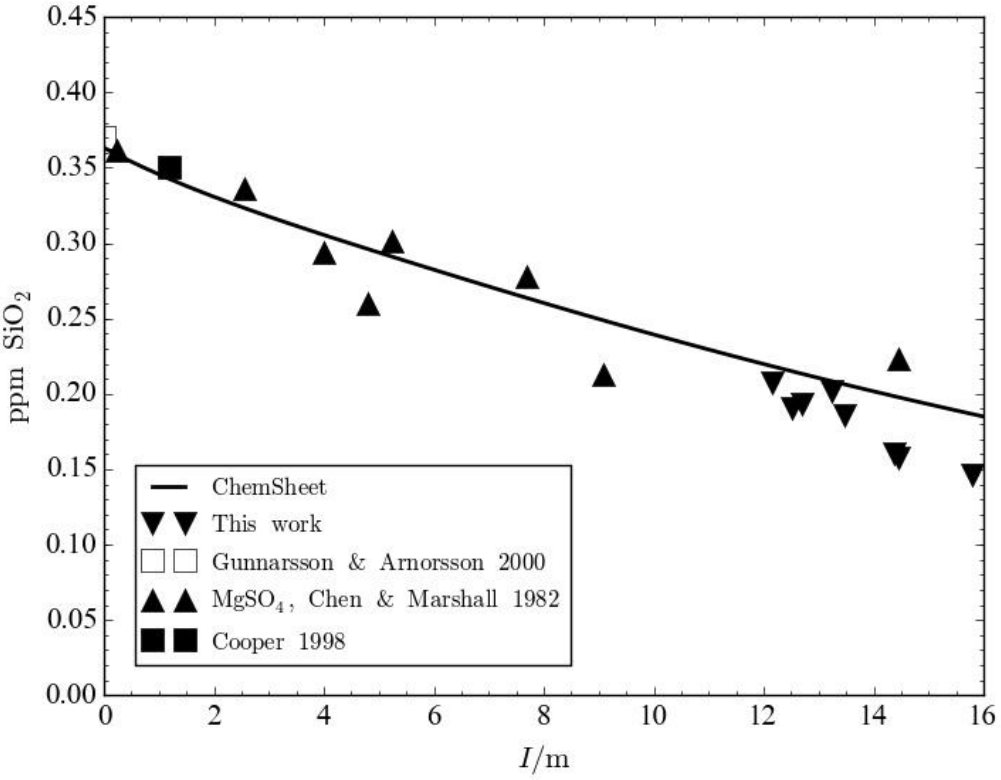
0.45
0.40
0.35
0.30
0.25
0.20
0.15
0.10
0.05
0.00
ppm SiO2
0
2
4
6
8
10
12
14
16
I/m
ChemSheet
This work
Gunnarsson & Arnorsson 2000
MgSO4, Chen & Marshall 1982
Cooper 1998

Figure 4

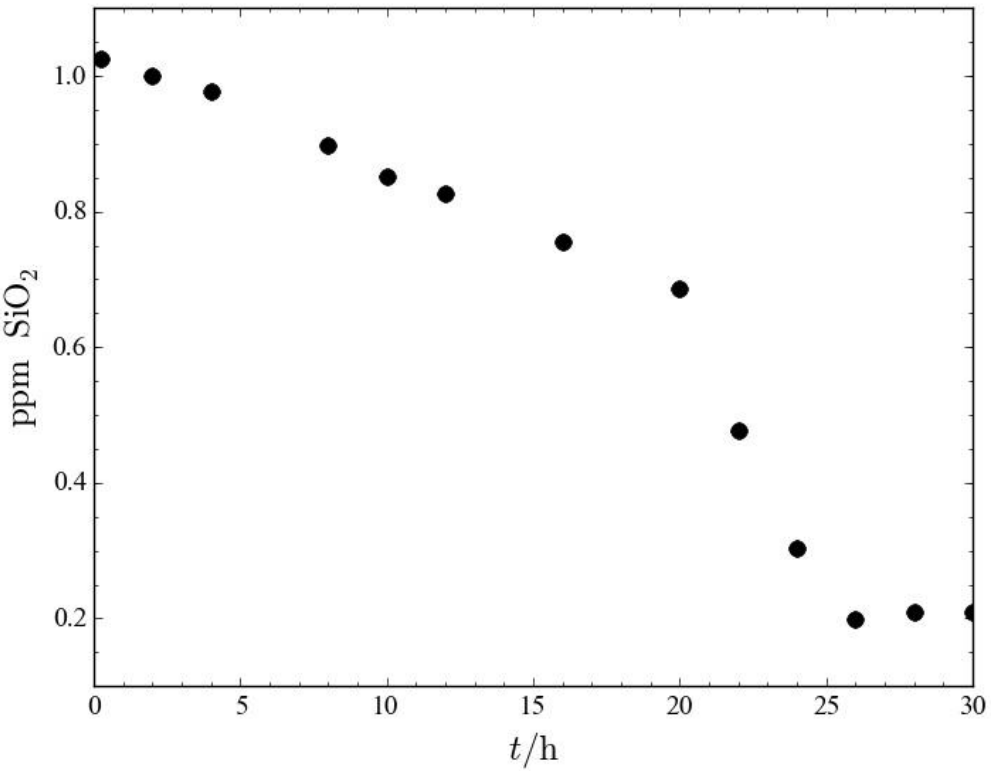

1 *Figure 5*

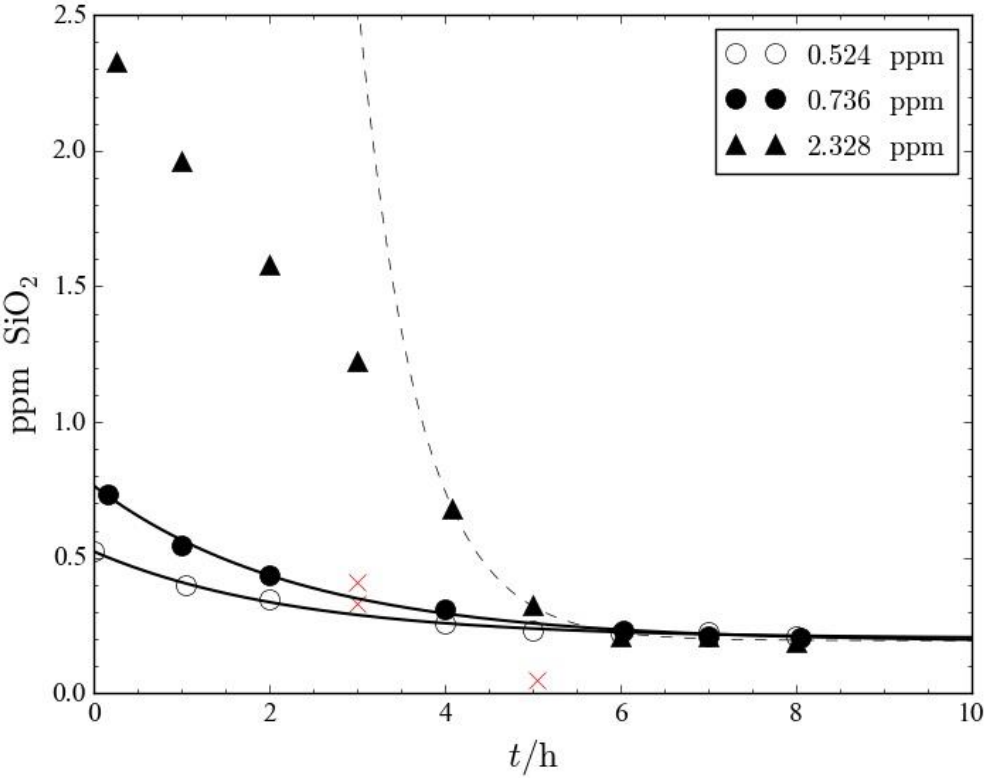

2

3

1 *Figure 6*

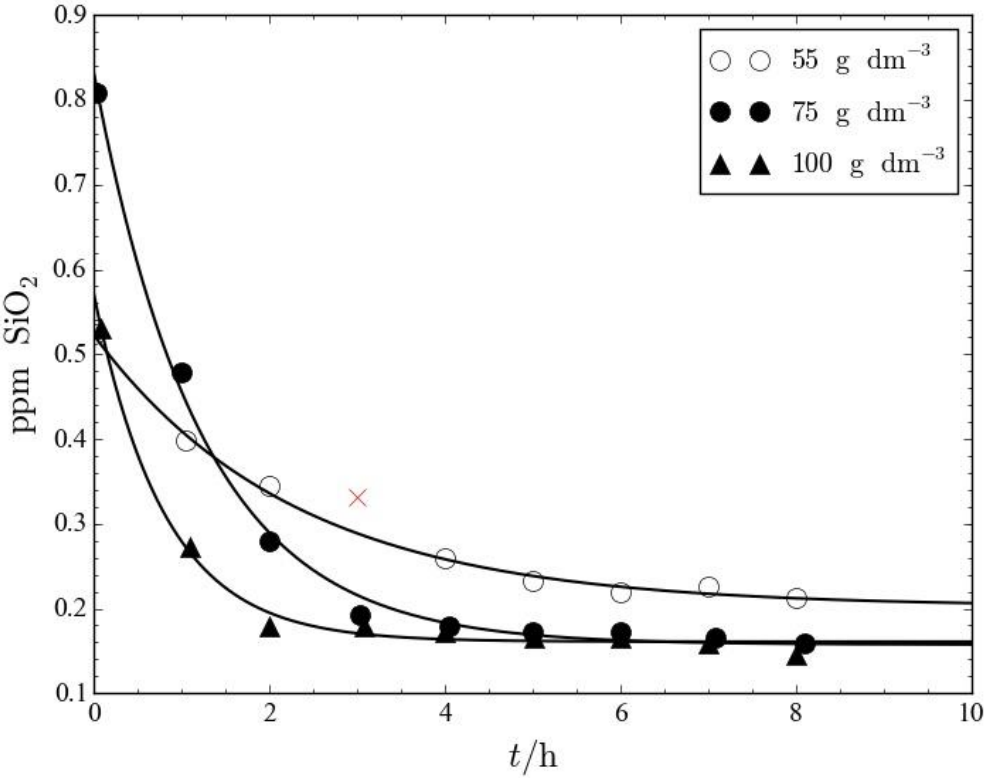
55 g dm^{-3}
75 g dm^{-3}
100 g dm^{-3}
ppm SiO$_2$
t/h
0.9
0.8
0.7
0.6
0.5
0.4
0.3
0.2
0.1
0
2
4
6
8
10

2

3

1 *Figure 7*

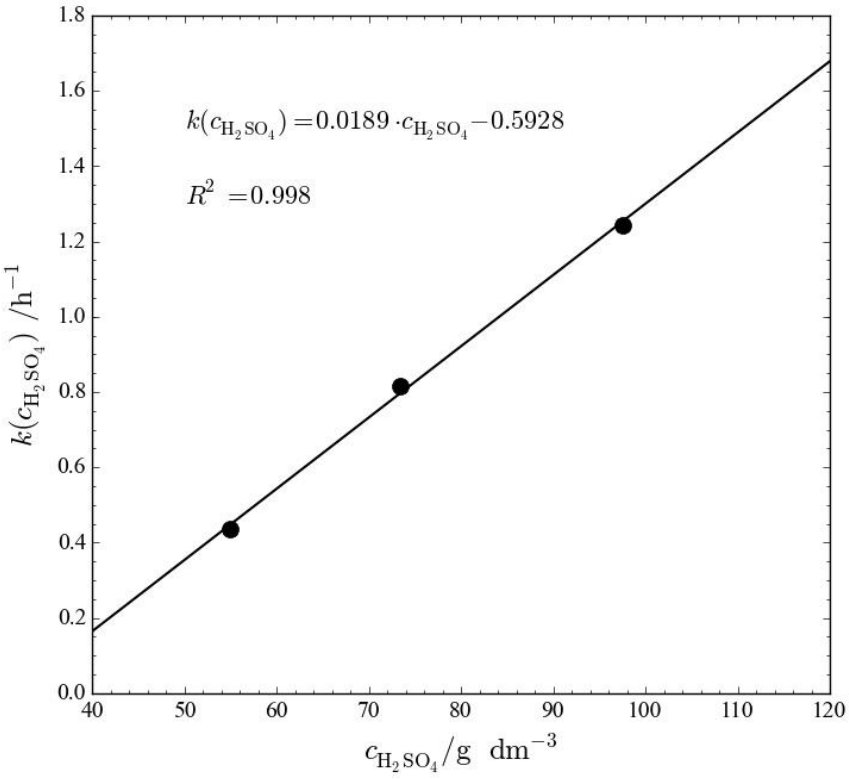
$k(c_{H_2SO_4}) = 0.0189 \cdot c_{H_2SO_4} - 0.5928$
$R^2 = 0.998$
$k(c_{H_2SO_4})\ /h^{-1}$
$c_{H_2SO_4}/g\ dm^{-3}$
0.0
0.2
0.4
0.6
0.8
1.0
1.2
1.4
1.6
1.8
40
50
60
70
80
90
100
110
120

2

3

1 *Figure 8*

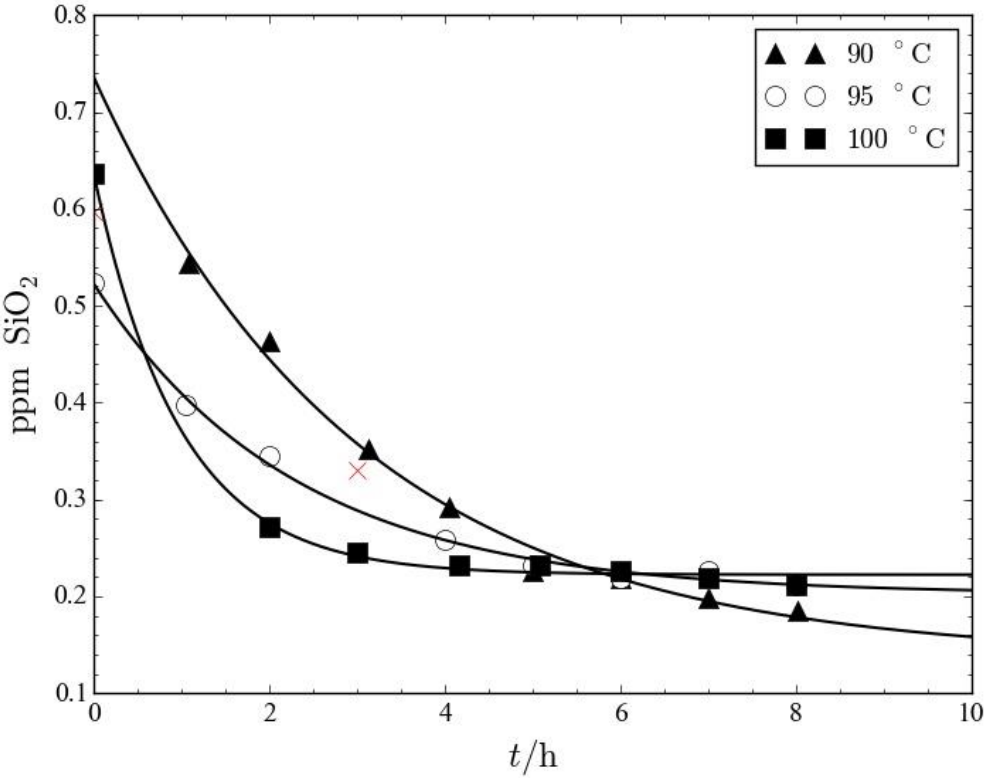

2

3

Figure 9

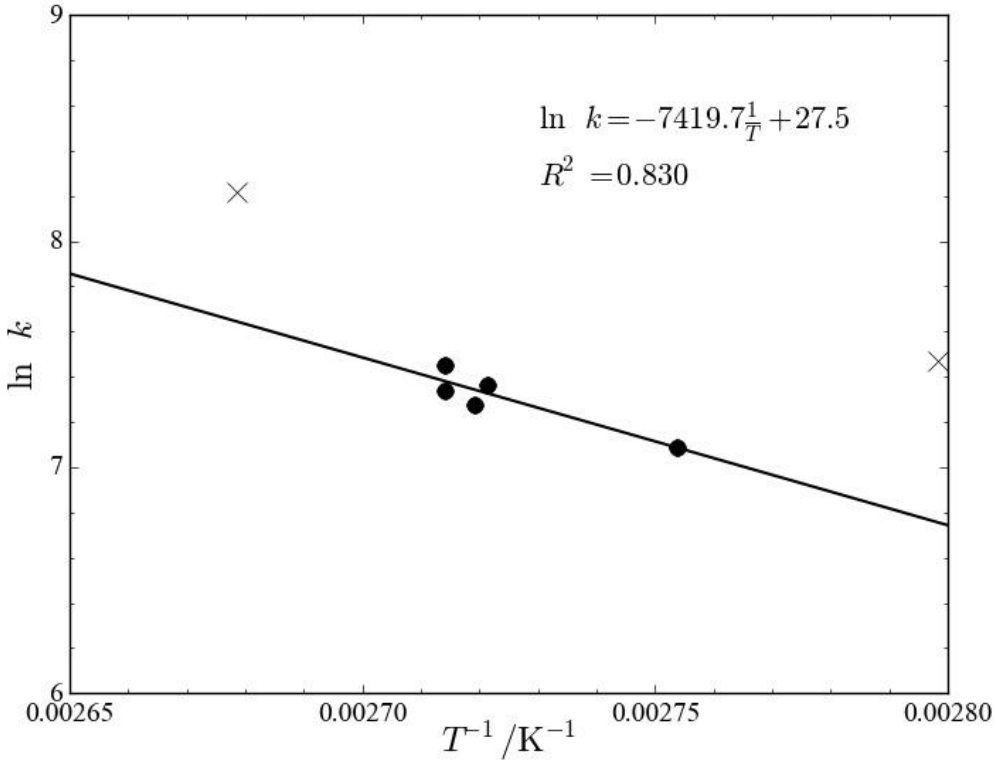
ln $k = -7419.7\frac{1}{T} + 27.5$
$R^2 = 0.830$
ln k
9
8
7
6
0.00265
0.00270
0.00275
0.00280
T^{-1} /K^{-1}

1 Graphical abstract

2

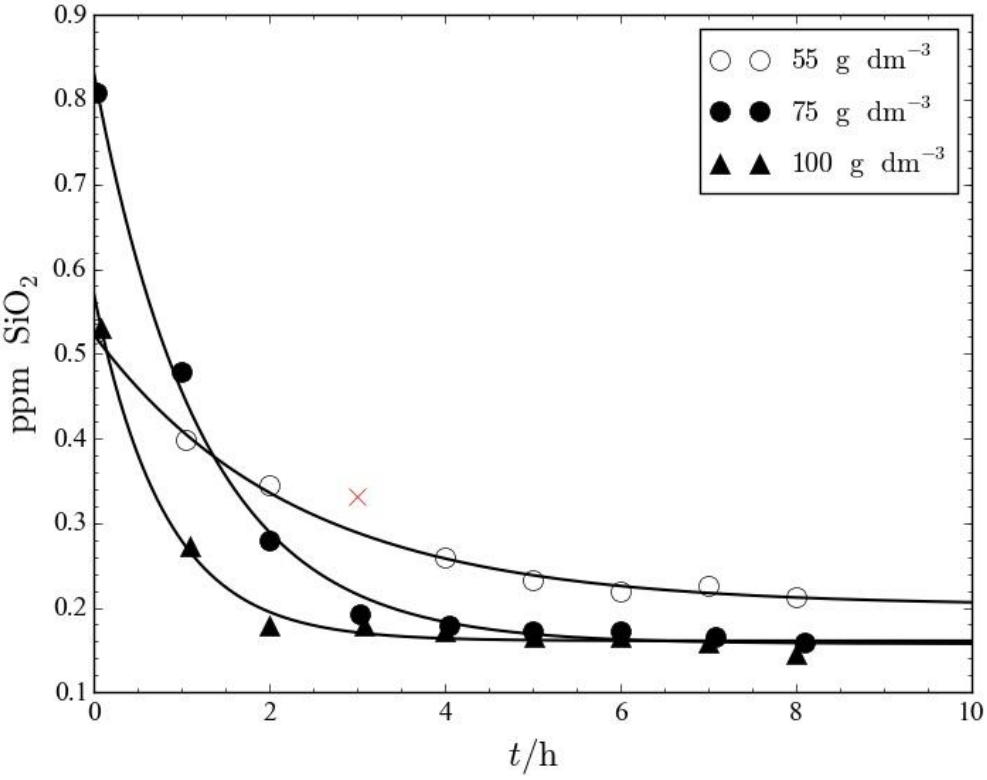

3